arXiv:0806.4163v1 [astro-ph] 25 Jun 2008

Submillimeter Observations of the Young Low-Mass Object IRAS 04158+2805

Sean M. Andrews[1,2], Michael C. Liu[3,4], Jonathan P. Williams[3], and K. N. Allers[3]

ABSTRACT

We present high spatial resolution Submillimeter Array observations and supplementary single-dish photometry of the molecular gas and dust around IRAS 04158+2805, a young source with spectral type M5-M6 in the Taurus star-forming region. A bright, highly elongated dust structure that extends $8''$ ($\sim$1120 AU) in diameter is revealed in a 883 μm thermal continuum image. This emission geometry is in good agreement with optical observations that show a similar structure in absorption, aligned perpendicular to bipolar scattered light nebulae. However, the interferometric data also clearly demonstrate that the submillimeter continuum emission is not centrally concentrated, but rather appears to have a toroidal geometry with substantially lower intensities inside a radius of $\sim$250-300 AU. Spatially resolved emission from the CO J=3$-$2 transition exhibits a velocity gradient along the major axis of the dust structure. If this kinematic pattern is interpreted as the signature of rotation around a central object, a relatively low mass is inferred ($M_* \sim 0.3\,M_\odot$, with a $\sim$50% uncertainty). We discuss several possible explanations for the observed gas and dust environment around IRAS 04158+2805, including a flattened envelope with an outflow cavity and a large circumbinary ring. This source offers unique views of the gas and dust environment surrounding a young low-mass stellar system. Its properties are generally not commensurate with formation scenarios for such low-mass objects that rely on dynamical ejection, but rather confirms that a single mechanism $-$ molecular cloud core collapse and fragmentation $-$ can produce stars over a wide range of stellar masses (at least an order of magnitude).

Subject headings: circumstellar matter — stars: formation — stars: low-mass, brown dwarfs — stars: pre-main-sequence — stars: individual (IRAS 04158+2805)

[1]Harvard-Smithsonian Center for Astrophysics, 60 Garden Street, Cambridge, MA 02138; sandrews@cfa.harvard.edu

[2]Hubble Fellow

[3]Institute for Astronomy, University of Hawaii, 2680 Woodlawn Drive, Honolulu, HI 96822; mliu@ifa.hawaii.edu, jpw@ifa.hawaii.edu, allers@ifa.hawaii.edu

[4]Alfred P. Sloan Research Fellow

1. Introduction

Circumstellar material profoundly influences the star formation process. A large-scale envelope acts as the local mass reservoir during the collapse and growth of a central protostar; a more compact disk regulates how that material is transported onto the star itself. A great deal of progress has been made in understanding the physical conditions present in the gas and dust surrounding Sun-like stars ($M_* \approx 0.5$-$3\,M_\odot$). However, it is unclear if those results can be extrapolated across the entire stellar mass spectrum. The low end of this spectrum ($M_* \leq 0.3\,M_\odot$) is of particular interest, as observations of the material around young low-mass objects[1] can help resolve an ongoing debate over their dominant formation mechanism.

The observed abundance of such low-mass objects relative to their more massive counterparts is difficult to account for with the traditional model for isolated star formation. Two distinct modifications have been proposed: (*a*) the turbulent fragmentation of cloud cores into smaller building units (e.g., Padoan & Nordlund 2004); and (*b*) a dynamical alternative where one component of a multiple system is ejected and prematurely cut off from its accretion reservoir (e.g., Reipurth & Clarke 2001; Umbreit et al. 2005). Both scenarios make distinct and conflicting predictions about the gas and dust environments that should be associated with low-mass objects. In the former, a disk/envelope structure similar to those noted around higher mass T Tauri stars would be expected. And for the latter, only a truncated disk (with an initial $R_d \lesssim 10\,\mathrm{AU}$) would survive the tidal stripping and ejection process (Bate et al. 2002). If the remnant material is sufficiently viscous, it could spread to radii up to $\sim$100 AU in $\sim$1 Myr (Armitage & Clarke 1997), but would have shed a vast majority of its initial mass in the ejection process. Therefore, observational constraints on the structure of the gas and dust around low-mass objects offer one avenue to help distinguish how they form.

A variety of observations demonstrate that the signatures of circumstellar gas and dust at small radii (up to a few AU) are indeed common for young low-mass objects (see the recent review by Luhman et al. 2007). More detailed individual studies confirm that such material has a geometry and composition similar to the disks around more massive T Tauri stars (Natta & Testi 2001; Pascucci et al. 2003; Allers et al. 2006; Bouy et al. 2008), although typically at lower masses (Klein et al. 2003; Scholz et al. 2006). However, these *unresolved* observations can not unambiguously constrain some key properties of this material, most significantly its spatial structure and extent.

In this article, we present new submillimeter observations of the molecular gas and dust surrounding IRAS 04158+2805. Located in the $\sim$1 Myr-old Taurus star-forming region, IRAS 04158+2805 has a cool central source with an estimated spectral type of M5-M6 (White & Hillenbrand 2004; Luhman 2006; Beck 2007). Recently, Glauser et al. (2008) provided an initial analysis of this

[1]For simplicity, we will refer to objects with $M_* \lesssim 0.3\,M_\odot$ as low-mass objects, including both very low-mass stars and brown dwarfs.

source and the dust structure surrounding it by modeling the broadband spectrum along with optical/infrared scattered light images. They suggested that their observations are best explained by a large (diameter of 2240 AU), massive (dust mass of 1-2$\times10^{-4}$ $M_\odot$; gas/dust ratio of 220^{+150}_{-170}) circumstellar disk around a low-mass star ($M_* \approx 0.1$-$0.2\,M_\odot$), with no need to include any contribution from a more extended envelope. Our new data represent the first high spatial resolution view of the gas and dust environment around this and similar cool, young objects at submillimeter wavelengths. They also provide an opportunity for a rare, albeit crude, estimate of M_* from the spatio-kinematics of circumstellar gas that is independent of pre-main-sequence evolution models. These observations are addressed in §2, and the resulting data products are highlighted in §3. In §4, we discuss the structure of the gas and dust surrounding IRAS 04158+2805 and what it can tell us about the central source and the formation of low-mass objects in general. The results are summarized in §5.

2. Observations and Data Reduction

Submillimeter interferometric observations of IRAS 04158+2805 ($\alpha = 4^{\rm h}18^{\rm m}58\overset{\rm s}{.}14$, $\delta = +28^\circ12'23\overset{''}{.}8$ [J2000]) were conducted in both the extended and compact configurations of the Submillimeter Array (SMA; Ho et al. 2004) on 2006 December 8 and 2007 January 27, respectively. In these configurations, the 8 SMA antennas (6 m diameter each) spanned baselines from ∼15-225 m. Double sideband receivers with a total bandwidth of 4 GHz were tuned to an effective continuum frequency of 339.9 GHz (883 μm). The correlator was simultaneously configured to observe the CO J=3−2 transition at 345.796 GHz at a spectral resolution of 0.70 km s^{-1}.

The observations cycled between IRAS 04158+2805 and two gain calibrators (3C111 and 3C84), with 20 minutes on target and 10 minutes on calibrator. The data were obtained in excellent observing conditions, with zenith optical depths at 225 GHz of 0.05-0.07. The raw visibilities were calibrated with the IDL-based MIR package.[2] Passband calibration was conducted with bright quasars (3C273, 3C279), and complex gain calibration was performed with 3C111. Using 3C84 as a consistency check on the gain solution, we estimate that phase noise generates an effective "seeing" of $<0\overset{''}{.}1$. Titan and Callisto were used to set the absolute flux scale, which is accurate to ∼10%. The MIRIAD package was utilized for the standard tasks of Fourier inversion, deconvolution, and imaging of the calibrated visibilities. Continuum and line maps from the combined datasets were made with natural weighting, providing a synthesized beam FWHM of $1\overset{''}{.}12 \times 0\overset{''}{.}86$ at a position angle of 92°.

IRAS 04158+2805 was also mapped at 450 and 850 μm using the jiggle-mode of the SCUBA camera at the 15 m James Clerk Maxwell Telescope (JCMT) on 2003 November 12 in dry, stable conditions ($\tau \approx 0.05$ at 225 GHz). Flux calibration accurate to ∼10% and 25% at 850 and 450 μm,

[2] `http://cfa-www.harvard.edu/$\sim$cqi/mircook.html`.

respectively, was achieved with observations of Neptune, and pointing was referenced to DG Tau and CRL 618. The bright emission, 0.44 ± 0.04 Jy at 850 μm and 1.6 ± 0.4 Jy at 450 μm, was not resolved at either wavelength in $15''$ and $9''$ beams, respectively. An additional map at 350 μm was obtained with the SHARC-II camera at the 10 m Caltech Submillimeter Observatory (CSO) on 2004 October 3 in similarly dry weather. Those data confirm an unresolved source ($9''$ beam) with a total flux density of 2.0 ± 0.5 Jy. All errors on flux densities include absolute calibration uncertainties (10% at 850 μm, and $\sim$25% at shorter wavelengths).

Optical images of IRAS 04158+2805 in the R-band were obtained with the University of Hawaii 2.2 m telescope on 2004 October 6. After the standard reduction of CCD data, the 7×300 s images were co-added and convolved with a 3-pixel ($0\farcs7$) FWHM Gaussian kernel to match the typical seeing for the observations and improve sensitivity to faint emission. The observations were not photometric.

3. Results

Images of the gas and dust surrounding IRAS 04158+2805 are shown in Figure 1. The optical R-band ($\sim$0.7 μm) image in Figure 1a reveals a high aspect ratio dark lane of *absorbing* material oriented roughly E-W (shown as grayscale-filled contours) that can be traced nearly $8''$ in diameter. First discovered by Glauser et al. (2008, see also Watson et al. 2007), this silhouette lane obscures the faint nebulosity associated with the nearby Herbig Ae star V892 Tau. Also pointed out by Glauser et al. (2008), the image in Figure 1a shows the conical nebulae perpendicular to the dark lane that are often produced by starlight scattered off the surface of flattened dust structures.

Figure 1b shows the first high resolution image of the thermal continuum emission from IRAS 04158+2805, at a wavelength of 883 μm. The morphology of that emission is remarkably similar to the optical silhouette, extending roughly $8''$ across, corresponding to a diameter of 1120 AU at the distance of the Taurus clouds ($d \approx 140$ pc; Elias 1978). Note that Glauser et al. (2008) trace I-band scattered light for this source to twice this diameter ($\sim 16''$, or 2240 AU). The difference compared to the R-band image in Figure 1a is related to the comparatively poor sensitivity of our observations, as was also noted for the infrared scattered light images in their study. Because the submillimeter emission was clearly unresolved in the 350 and 450 μm maps, we can infer that it has a diameter of $\leq 9''$ (1260 AU). The absence of very short antenna spacings implies that the interferometric observations have significantly diminished sensitivity to structures larger than $\sim 10''$ (e.g., Wilner & Welch 1994). Therefore, because of the diminished sensitivity to faint submillimeter emission on large scales, there is no reason to suspect that the sized inferred here is physically inconsistent with the scattered light image presented by Glauser et al. (2008). The integrated flux density at 883 μm is 407 ± 41 mJy, consistent with the SCUBA measurement. A fit of the SMA visibilities with an elliptical Gaussian model indicates an inclination of $62 \pm 3^\circ$ (where 90° corresponds to edge-on) at a position angle of $93 \pm 1^\circ$ (measured east of north), in excellent agreement with the constraints imposed by modeling the scattered light (Glauser et al. 2008). Fits with a ring

or pedastal emission model give the same results.

The high surface brightness at large distances from the central source and large spatial extent of the continuum emission are fairly unique. The steep drop of the visibilities over a short range of baseline lengths, as shown in Figure 2, indicates that essentially all of the emission is concentrated at large spatial scales (radii $\gtrsim 250$ AU). More significantly, the visibilities show a pronounced null at $\sim$30-40 kλ and very little flux on longer baselines. These are definitive signatures of a brightness distribution with a central "hole", inside of which there is significantly diminished intensity. Assuming a simple ring geometry, the location of the null suggests an inner radius of $\sim$250-300 AU (e.g., Hughes et al. 2007). Asymmetries in the submillimeter map confirm this geometry, with emission peaks centered roughly $\pm 1\farcs9$ ($\sim$265 AU) from the image center. The western lobe is approximately 50% brighter than the eastern lobe. These asymmetries are real, as they are clearly detected in 3 separate observing runs at the same location and intensity (the 2 detailed here, and the hybrid compact/extended observations described by Andrews & Williams 2007a)[3].

A velocity-integrated intensity ($0^{\rm th}$ moment) map of the CO J=3−2 emission from IRAS 04158+2805 is shown in Figure 1c. The CO emission morphology is significantly different than the optical silhouette and submillimeter continuum, occupying a region $\sim 4''$ on a side with a central, slightly elongated peak. The integrated intensity is 40.7 ± 0.4 Jy km s^{-1} (using 9 channels for a total width of 6.3 km s^{-1}). Fainter CO emission extends above and below the plane of the continuum emission in an "X"-shaped pattern out to $\sim 2''$ from the image center. There is a steep drop in the CO intensity along the plane of the silhouette that corresponds precisely to the positions of the submillimeter continuum peaks described above. The kinematic structure of the CO associated with IRAS 04158+2805 is exhibited in Figure 3. These channel maps clearly show a CO velocity gradient along the major axis of the continuum emission and silhouette (i.e., in the east-west direction), similar to the pattern expected for rotation around a central source.

4. Discussion

4.1. The Central Object

Estimating the masses of young stars and brown dwarfs generally requires reference to theoretical models of their structural evolution. The quantitative reliability of such models for individual stars at ages $\lesssim$1 Myr is highly uncertain, particularly for the low end of the stellar mass spectrum where complicated convection physics, dusty atmospheres, and uncertain molecular opacities and initial conditions can strongly affect the observational diagnostics (e.g., D'Antona & Mazzitelli 1994; Baraffe et al. 2002; Montalbán et al. 2004). Dynamical constraints on M_* from the orbital properties of either a companion star (e.g., Mathieu 1994) or gas in a circumstellar disk (e.g.,

[3]In fact, the image made from the hybrid configuration in Andrews & Williams (2007a) shows *only* the western peak of this asymmetry, and heavily resolves the remainder of the emission.

Simon et al. 2000) provide an extremely valuable independent check that can potentially be used to calibrate these models (see Hillenbrand & White 2004). Stassun et al. (2006) report the only such measurements of young ∼M6 dwarfs to date, for an eclipsing binary system in Orion. With the first spatially resolved measurements of molecular gas in apparent rotation around a young low-mass object with similar spectral type, the CO observations of IRAS 04158+2805 presented here can provide another such estimate of M_*, although admittedly with a great deal more uncertainty.

Figure 4 shows the position-velocity diagram of the CO J=3−2 line emission for IRAS 04158+2805, where the angular offset is the distance from the observed phase center (such that positions to the east have positive values) and the velocity offset is taken relative to the systemic value ($V_* = 7.4\,\mathrm{km\ s^{-1}}$). Overlaid on the diagram is an inclined ($i = 62°$) Keplerian rotation profile that matches the general kinematic trend in the data rather well (thick curve), with a central point mass of $M_* = 0.30\,\mathrm{M_\odot}$. Additional rotation profiles for $M_* = 0.15$ and $0.45\,\mathrm{M_\odot}$ are also shown for reference. It should be noted that these profiles assume pure Keplerian orbital motion around a central source, which may not be the case in the more complex IRAS 04158+2805 environment. For now, we assume that the dominant kinematic trend is such rotation, but potential complications will be addressed below.

A comparison of this dynamical M_* estimate with predictions from stellar evolution models is a challenge because of uncertainties in the luminosity (due to scattered light contamination at short wavelengths), extinction, and effective temperature for the central source. Recent analysis of the scattered light spectrum from IRAS 04158+2805 suggest that this source is cool, with initial spectral type estimates of M6±1 (White & Hillenbrand 2004; Beck 2007) refined to M5.25±0.25 (optical) and M6±0.5 (infrared; Luhman 2006).[4] Using the latter classifications and the Luhman et al. (2003) empirical effective temperature scale, we estimate $T_* = 3050 \pm 75\,\mathrm{K}$. Unfortunately, large uncertainties in the extinction, where estimates range from $A_V \approx$ 9-16 (e.g., White & Hillenbrand 2004; Beck 2007), make a luminosity determination difficult. However, we can use pre-main-sequence models for an assumed age in the inferred temperature range to estimate a central mass. Using the T_* range quoted above and an age of ∼1 Myr, the D'Antona & Mazzitelli (1997) and Baraffe et al. (1998) models indicate $M_* \approx 0.09$-$0.16\,\mathrm{M_\odot}$. This mass range does not include the additional uncertainties on the adopted effective temperature scale or the unknown age of the source.

The M_* values inferred from the pre-main-sequence models lie roughly a factor of 2 below the nominal value that best describes the kinematics of the CO gas inferred above. The unquoted and poorly understood uncertainties in both measurements may be the simple explanation for this apparent discrepancy. Without a detailed physical model for the local gas structure around IRAS 04158+2805, it is difficult to estimate a statistically acceptable range of M_* from the CO kinematics; there may very well be overlap with the higher end of the M_* range from the pre-main-sequence models. The effective temperature scale adopted above is also uncertain. A ∼500 K increase in the effective temperature (to a value that is typically associated with M2 stars) would reconcile the

[4]Note that previous spectral type assignments ranged from ∼K7 to M3 (Kenyon et al. 1998; Luhman 1999).

M_* estimates. Indeed, using an independent method of fitting infrared spectra, Doppmann et al. (2005) infer $T_* = 3500\,\mathrm{K}$ for the IRAS 04158+2805 central source, leading to $M_* \approx 0.35$-$0.45\,\mathrm{M}_\odot$ in the aforementioned models. Moreover, Hillenbrand & White (2004) have shown that pre-main-sequence models generally tend to underpredict M_* compared to dynamical measurements in this low-mass range, although typically only by $\leq 20\%$. In their recent study that explicitly includes the effects of scattered starlight, Glauser et al. (2008) argue for a very luminous central source, $L_* \approx 0.4\,\mathrm{L}_\odot$. While this value must be somewhat degenerate with the dust properties and structure assumed in their model, it is clearly the most robust estimate available. The pre-main-sequence models imply that such a luminous cool source would be very young, with an age significantly less than 1 Myr. The model mass tracks at such ages are not well understood in light of the uncertain initial conditions.

Clearly, the aforementioned uncertainties can be solely responsible for the apparently different M_* estimates from the CO kinematics and pre-main-sequence models. Alternatively, there is also an appealing and simple physical explanation – the IRAS 04158+2805 central source may be a roughly equal-mass binary. In this scenario, the M_* estimate from the CO kinematics refers to the total mass of the stellar system (i.e., the mass interior to the gas that produces the line emission), while the estimate from the pre-main-sequence models assumes only a single star. Therefore we would expect to see both a high luminosity (as claimed by Glauser et al. 2008) and $M_*(\mathrm{CO}) \sim 2M_*(\mathrm{models})$. A variety of surveys suggest that such binaries are fairly common, $\sim$35-45% for M dwarfs (Fischer & Marcy 1992; Reid & Gizis 1997) and $\sim$10-30% for cooler objects (e.g., Burgasser et al. 2007). While it is difficult to definitively state the properties of the central source(s), we can further assess the nature of IRAS 04158+2805 by analyzing the structure of the material that surrounds it.

4.2. The Gas and Dust Environment

Given the elongated structures shown in Figure 1, it is reasonable to suggest that the gas and dust around IRAS 04158+2805 reside in an exceptionally large circumstellar disk. Glauser et al. (2008) have recently demonstrated that they are able to fit high-quality scattered light images and the SED for this source with a simple disk structure, and without the need to invoke any envelope component. With the new data presented here, it is worthwhile to re-examine the structure of this material.

IRAS 04158+2805 is exceptionally bright at submillimeter wavelengths, with an $850\,\mu$m luminosity larger than $\sim$85% of all other sources detected in the Andrews & Williams (2005) Taurus survey. Breaking that sample down further, the IRAS 04158+2805 submillimeter emission is brighter than $\sim$90% of Class II sources (disk only), but is comparable to the median Class I source (disk + envelope). If we adopt the standard emissivity for disks ($0.034\,\mathrm{cm}^2\ \mathrm{g}^{-1}$ at $883\,\mu$m, including a gas-to-dust ratio of 100) and assume that the submillimeter continuum emission is optically thin and has a characteristic temperature of $\sim$20 K (e.g., Beckwith et al. 1990; Andrews & Williams

2005, 2007b), the integrated SMA flux density suggests a large total mass of gas and dust is present around IRAS 04158+2805, $\sim$0.03 $M_\odot$. This value is in good agreement with the disk mass range inferred by Glauser et al. (2008), $M_d \approx$ 0.02-0.04 $M_\odot$. Estimating masses for circumstellar material in this way is inherently uncertain (perhaps by an order of magnitude), due to the challenge of observationally constraining the optical properties of dust grains and the assumed mass conversion of a trace constituent (dust) to the presumably dominant species (molecular gas).

Perhaps more compelling (and easier to interpret) is the unusual geometry that is observed for the dust structure around IRAS 04158+2805. The enormous size of the scattered light nebulae noted by Glauser et al. (2008, 2240 AU diameter) and the submillimeter continuum emission presented here (1120 AU diameter) is exceptionally rare for circumstellar disks (e.g., Piétu et al. 2007; Watson et al. 2007; Andrews & Williams 2007a; Hughes et al. 2008), rivaled only by the circumbinary disk around UY Aur (Duvert et al. 1998; Close et al. 1998; Potter et al. 2000). On the contrary, the observed size is fairly typical (if not on the small end) for larger-scale envelopes (e.g., Looney & Mundy 2000; Eisner et al. 2005).

Moreover, our resolved observations of the submillimeter continuum reveal that a large central region (perhaps $\sim$500 AU in diameter) has significantly diminished intensity at 883 μm, suggesting a ring-like or toroidal geometry for the dust structure. Similar geometries have been inferred for a handful of circumstellar disks, and a variety of underlying causes are possible. The so-called "transition" disks have their inner regions (out to a few tens of AU in radius) largely cleared of observable material, presumably by disk evolution processes like particle growth, photoevaporation, or dynamical interactions with a young planetary system (e.g., Piétu et al. 2006; Hughes et al. 2007; Brown et al. 2008). However, given the large spatial scale of the central depression and the absence of a corresponding dip in the infrared part of the IRAS 04158+2805 SED, as shown in Figure 5, this scenario is unlikely.

Alternatively, extremely dense disks with edge-on orientations can potentially render even the submillimeter emission optically thick, resulting in a central depression in its brightness distribution (e.g., Wolf et al. 2008). Although the IRAS 04158+2805 dust structure is not oriented edge-on, perhaps longer pathlengths through the exceptionally large structure can provide compensating column densities. If the bulk of the submillimeter emission is optically thick, the spectrum should have a spectral index $\alpha = 2$, where $F_\nu \propto \nu^\alpha$ (Beckwith & Sargent 1991). Power-law fits to the submillimeter photometry are significantly steeper than the optically thick case, with $\alpha = 2.7 \pm 0.3$ (0.45-1.3 mm; $\alpha = 3.8 \pm 0.6$ for 0.85-1.3 mm). At these wavelengths, such a steep spectrum is only noted for a few percent of Class II sources in Taurus and ρ Oph, but is more common (25-35%) in the envelopes around Class I objects (Andrews & Williams 2005, 2007b). The observed steep submillimeter SED would be difficult to produce unless a large fraction of the dust was optically thin at those wavelengths. As noted by Wolf et al. (2008), a clear test of this possibility can be made with resolved continuum observations at $\lambda > 883\,\mu$m. In such data, the material should become optically thick only at significantly smaller radii than at 883 μm, resulting in a more centrally concentrated emission profile (or, equivalently, the null in the visibilities should be detected at a comparatively

longer deprojected baseline). Note that if the material inside this central depression is optically thick at 883 μm, an enormous reservoir of mass is not accounted for in the above estimate.

A third possibility for explaining the submillimeter continuum depression is that the emitting dust resides in a circumbinary ring. The material around close binary stars is expected to be dynamically cleared on scales similar to the physical separation of the stellar components (e.g., Jensen et al. 1996; Guilloteau et al. 1999).[5] Numerical simulations of this dynamical interaction suggest that a circumbinary disk gap would be cleared out to a radius $\sim$1.5-3$\times$ the projected semimajor separation of the stellar components, and the individual circumstellar disks would be truncated at a radius $\sim$0.2-0.5$\times$ the projected semimajor separation (e.g., Artymowicz & Lubow 1994). If the 883 μm continuum depression noted here is caused by such clearing, we would expect the projected binary separation to be $\sim$90-180 AU ($\sim$0.″6-1.″3) for a reasonable range of eccentricities, and the remnant individual circumstellar disks might be truncated at radii of $\sim$20-90 AU. This configuration is similar to the UY Aur system, where a ring with $\sim$20″ diameter is detected in both scattered light and CO around a roughly equal-mass binary with a similar projected separation (Duvert et al. 1998; Close et al. 1998; Potter et al. 2000). The primary difference is in the masses involved; the stellar mass in the IRAS 04158+2805 system is $\sim$4$\times$ less than for UY Aur, but the circumstellar mass (or rather 850 μm luminosity) is $\sim$4$\times$ higher. While this possibility is certainly appealing in its reconciliation of both the information on the central source (see §4.1) and the structure of the gas and dust emission, testing the multiplicity of IRAS 04158+2805 will be a challenge given the obscuration of the central region by the dust structure. Decomposing high resolution spectra of scattered starlight may represent the best opportunity in this case.

The IRAS 04158+2805 SED, shown in Figure 5, exhibits a strong infrared excess with a flat or slightly rising slope from 2-25 μm. A variety of solid-state absorption features are noted in higher resolution infrared spectra, including H_2O ice (3 μm; not shown), silicates (10 μm), and CO_2 ice (15 μm; Beck 2007; Furlan et al. 2008). The bright and steep submillimeter spectrum has already been discussed above. While all of these SED properties are not necessarily inconsistent with a large, cold, highly inclined circumstellar disk (e.g., Men'shchikov & Henning 1997; Chiang & Goldreich 1999; Pontoppidan et al. 2005), taken together they are more common for Class I/Flat-Spectrum objects that harbor a remnant accretion envelope (e.g., Whitney et al. 2003; Watson et al. 2004; Boogert et al. 2004; Pontoppidan et al. 2007). Furlan et al. (2008) demonstrate that the IRAS 04158+2805 SED features are strikingly similar to those for several other Class I sources in Taurus (see their Fig. 2) and can be successfully reproduced in detail with an envelope model (although the new observations of this source warrant a modification of their geometric assumptions). So, all of the observational evidence presented here is also consistent with a flattened envelope structure around IRAS 04158+2805. Such a flattened envelope geometry is predicted by molecular cloud

[5]Recent observations suggest that the circumbinary scenario may be the more appropriate explanation in some cases for the diminished central emission in both transition (Ireland & Kraus 2008) and dense, edge-on disks (Guilloteau et al. 2008).

core collapse models that incorporate rotation or magnetic fields (Terebey et al. 1984; Galli & Shu 1993), and have been clearly detected in other cases, albeit on significantly larger spatial scales than noted here (e.g., Looney et al. 2007).

In this scenario, a partially evacuated outflow cavity at the center of the flattened envelope may explain the central depression in the submillimeter continuum data (e.g., Whitney et al. 2003, their Models 3 or 4). Glauser et al. (2008) indicate that IRAS 04158+2805 drives a substantial Hα jet oriented in the north-south direction, perpendicular to the observed dust structure. The velocity-integrated CO J=3−2 morphology does resemble the bases of some molecular outflows (e.g., Arce & Sargent 2006), but the absence of both a velocity gradient in the proposed flow direction (north-south) and larger scale molecular outflow signatures (Bontemps et al. 1996; Gomez et al. 1997) are difficult to reconcile with that interpretation. Nevertheless, some contribution to the CO emission from an outflow and even the envelope (i.e., motions unrelated to Keplerian rotation) would complicate the observed spatio-kinematics. The dynamical estimate of M_* discussed above should be treated with caution with regards to this possibility. Of course, the envelope and binary ideas are not mutually exclusive, and dynamical clearing of the inner envelope and disks is still a viable alternative.

The images in Figures 1c and 3 demonstrate that, unlike the submillimeter continuum, the CO emission is centrally concentrated; most of the line emission is from radii inside the toroidal structure traced in the continuum. While this may suggest that the bulk of the line emission is generated in the disk(s) interior to that structure, it is difficult to provide a reliable origin without a more complete physical model for the IRAS 04158+2805 environment. Future studies of this source should focus on searching for definitive molecular outflow signatures, resolving dense gas tracers that are commonly associated with envelopes (e.g., Jørgensen et al. 2007), observing CO transitions at higher spectral resolution to provide a better tracer of the velocity field, and reconciling the optical/near-infrared scattered light observations with the submillimeter results in an effort to converge on a consistent model of the local gas and dust structure.

Considering the low stellar mass range implied for IRAS 04158+2805, it is difficult to reconcile the large mass reservoir and size of this environment with any formation scenario that relies on it being dynamically ejected from a more massive system (e.g., Reipurth & Clarke 2001; Bate et al. 2002). Rather, the observed gas and dust structure is more consistent with the standard scenario, where an accretion disk and perhaps a remnant envelope developed around a single (or binary) source during the gravitational collapse of a molecular cloud core fragment. Regardless of the precise value of M_*, IRAS 04158+2805 is a remarkable example of the fact that the standard picture for star formation worked out for higher-mass stars is also applicable at the low end of the stellar mass function.

5. Summary

We have presented new submillimeter observations of the molecular gas and dust around IRAS 04158+2805, a young low-mass object in the Taurus star-forming region. The data reveal a complex and surprising environment, from which we infer the following:

1. A high aspect ratio ($i \approx 62°$) dust structure with a projected diameter of ∼1120 AU and estimated (gas+dust) mass of ∼0.03 $M_\odot$ is noted in optical absorption and submillimeter continuum emission images. The resolved 883 μm data clearly demonstrate a central depression in the emission, suggesting a ring-like geometry with an inner radius of ∼250-300 AU. A variety of structures that may explain the observations are investigated, with a flattened envelope or circumbinary ring perhaps the most likely.

2. Spatially resolved CO J=3−2 line emission shows a velocity gradient along the major axis of the dust structure. Assuming the gas traced by this transition is in Keplerian orbital motion around a central source, the spatio-kinematic properties of the emission are used to estimate a central mass, $M_* \approx 0.3\,M_\odot$ (with ∼50% uncertainty). This estimate is roughly a factor of 2 higher than the mass range inferred from a reasonable effective temperature range and pre-main-sequence models, ∼0.09-0.16 $M_\odot$, but the significant uncertainties on both measurements do not formally rule out their mutual consistency. However, a roughly equal-mass binary system represents an intriguing possibility in this case, as it would naturally account for this possible M_* discrepancy, a very high luminosity, and the ring-like geometry of the dust structure.

3. The large spatial extent and mass of the complex gas and dust environment surrounding IRAS 04158+2805 would be difficult to retain in the dynamical ejection models used to explain the formation of such low-mass objects. Instead, this case appears to illustrate that the standard gravitational collapse models applied to stars with masses up to ∼2-3 $M_\odot$ can be extrapolated down to objects with $M_* \sim$ 0.1-0.3 $M_\odot$. More detailed models of the IRAS 04158+2805 gas and dust structure and specialized observations are recommended.

We thank F. Ménard and G. Duchêne for encouraging our interest in this source, and Elise Furlan for kindly providing the mid-infrared spectrum. We are grateful to an anonymous referee for a helpful, constructive review and for emphasizing the potential circumbinary nature of IRAS 04158+2805. The SMA is a joint project between the Smithsonian Astrophysical Observatory and the Academia Sinica Institute of Astronomy and Astrophysics and is funded by the Smithsonian Institution and the Academia Sinica. Support for this work was provided by NASA through Hubble Fellowship grant #HF-01203.01-A awarded by the Space Telescope Science Institute, which is operated by the Association of Universities for Research in Astronomy, Inc., for NASA, under contract NAS 5-26555. MCL and KNA acknowledge support for this work from NSF grant AST-0407441.

REFERENCES

Allers, K. N., Kessler-Silacci, J. E., Cieza, L. A., & Jaffe, D. T. 2006, ApJ, 644, 364

Andrews, S. M., & Williams, J. P. 2005, ApJ, 635, 1134

——— 2007, ApJ, 659, 705 (2007a)

——— 2007, ApJ, 671, 1800 (2007b)

Arce, H. G., & Sargent, A. I. 2006, ApJ, 646, 1070

Armitage, P. J., & Clarke, C. J. 1997, MNRAS, 285, 540

Artymowicz, P., & Lubow, S. H. 1994, ApJ, 421, 651

Baraffe, I., Chabrier, G., Allard, F., & Hauschildt, P. H. 1998, A&A, 337, 403

———, 2002, A&A, 382, 563

Bate, M. R., Bonnell, I. A., & Bromm, V. 2002, MNRAS, 332, L65

Beck, T. L. 2007, AJ, 133, 1673

Beckwith, S. V. W., Sargent, A. I., Chini, R., & Güsten, R. 1990, AJ, 99, 924

Beckwith, S. V. W., & Sargent, A. I. 1991, ApJ, 381, 250

Beichman, C. A., et al. 1986, ApJ, 307, 337

Bontemps, S., André, P., Terebey, S., & Cabrit, S. 1996, A&A, 311, 858

Boogert, A. C., et al. 2004, ApJS, 154, 359

Bouy, H., et al. 2008, A&A, in press (astro-ph/0803.2051)

Brown, J. M., Blake, G. A., Qi, C., Dullemond, C. P., & Wilner, D. J. 2008, ApJ, 675, L109

Burgasser, A. J., Reid, I. N., Siegler, N., Close, L., Allen, P., Lowrance, P., & Gizis, J. 2007, in Protostars & Planets V, eds. B. Reipurth, D. Jewitt, & K. Keil (Univ. Arizona Press: Tucson), 427

Chiang, E. I., & Goldreich, P. 1999, ApJ, 519, 279

Close, L. M., et al. 1998, ApJ, 499, 883

Cutri, R. M., et al. 2003, 2MASS All-Sky Point Source Catalog (Pasadena: IPAC)

D'Antona, F., & Mazzitelli, I. 1994, ApJS, 90, 467

——— 1997, Mem. Soc. Astron. Italiana, 68, 807

Doppmann, G. W., Greene, T. P., Covey, K. R., & Lada, C. J. 2005, AJ, 130, 1145

Duvert, G., Dutrey, A., Guilloteau, S., Ménard, F., Schuster, K., Prato, L., & Simon, M. 1998, A&A, 332, 867

Eisner, J. A., Hillenbrand, L. A., Carpenter, J. M., & Wolf, S. 2005, ApJ, 635, 396

Elias, J. H. 1978, ApJ, 224, 857

Fischer, D., & Marcy, G. 1992, ApJ, 396, 178

Furlan, E., et al. 2008, ApJS, 176, 184

Galli, D., & Shu, F. H. 1993, ApJ, 417, 220

Glauser, A. M., Ménard, F., Pinte, C., Duchêne, G., Güdel, M., Monin, J.-L., & Padgett, D. L. 2008, A&A, in press (astro-ph/0804.3483)

Gomez, M., Whitney, B. A., & Kenyon, S. J. 1997, AJ, 114, 1138

Guilloteau, S., Dutrey, A., & Simon, M. 1999, A&A, 348, 570

Guilloteau, S., Dutrey, A., Pety, J., & Gueth, F. 2008, A&A, 478, L31

Hillenbrand, L. A., & White, R. J. 2004, ApJ, 604, 741

Ho, P. T. P., Moran, J. M., & Lo, K. Y. 2004, ApJ, 616, L1

Hughes, A. M., Wilner, D. J., Calvet, N., D'Alessio, P., Claussen, M. J., & Hogerheijde, M. R. 2007, ApJ, 664, 536

Hughes, A. M., Wilner, D. J., Qi, C., & Hogerheijde, M. R. 2008, ApJ, 678, 1119

Ireland, M. J., & Kraus, A. L. 2008, ApJ, 678, L59

Jensen, E. L. N., Mathieu, R. D., & Fuller, G. A. 1994, ApJ, 429, L29

Jørgensen, J. K., et al. 2007, ApJ, 659, 479

Kenyon, S. J., Brown, D. I., Tout, C. A., & Berlind, P. 1998, AJ, 115, 2491

Klein, R., Apai, D., Pascucci, I., Henning, T., & Waters, L. B. F. M. 2003, ApJ, 593, L57

Lay, O. P., Carlstrom, J. E., & Hills, R. E. 1997, ApJ, 489, 917

Looney, L. W., & Mundy, L. G. 2000, ApJ, 529, 477

Looney, L. W., Tobin, J. J., & Kwon, W. 2007, ApJ, 670, L131

Luhman, K. L. 1999, ApJ, 525, 466

——— 2006, ApJ, 645, 676

Luhman, K. L., Stauffer, J. R., Muench, A. A., Rieke, G. H., Lada, E. A., Bouvier, J., & Lada, C. J. 2003, ApJ, 593, 1093

Luhman, K. L., et al. 2006, ApJ, 647, 1180

Luhman, K. L., Joergens, V., Lada, C., Muzerolle, J., Pascucci, I., & White, R. 2007, in Protostars & Planets V, eds. B. Reipurth, D. Jewitt, & K. Keil (Univ. Arizona Press: Tucson), 443

Luhman, K. L., & Rieke, G. H. 1998, ApJ, 497, 354

Mathieu, R. D. 1994, ARA&A, 32, 465

Men'shchikov, A. B., & Henning, T. 1997, A&A, 318, 879

Montalbán, J., D'Antona, F., Kupka, F., & Heiter, U. 2004, A&A, 416, 1081

Motte, F., & André, P. 2001, A&A, 365, 440

Natta, A., & Testi, L. 2001, A&A, 376, L22

Pascucci, I., Apai, D., Henning, T., & Dullemond, C. P. 2003, ApJ, 590, L111

Padoan, P., & Nordlund, Å. 2004, ApJ, 617, 559

Piétu, V., Dutrey, A., Guilloteau, S., Chappilon, E., & Pety, J. 2006, A&A, 460, L43

Piétu, V., Dutrey, A., & Guilloteau, S. 2007, A&A, 467, 163

Pontoppidan, K. M., et al. 2005, ApJ, 622, 463

——— 2008, ApJ, 678, 1005

Potter, D. E., et al. 2000, ApJ, 540, 422

Reid, I. N., & Gizis, J. 1997, AJ, 113, 2246

Reipurth, B., & Clarke, C. 2001, AJ, 122, 432

Scholz, A., Jayawardhana, R., & Wood, K. 2006, ApJ, 645, 1498

Simon, M., Dutrey, A., & Guilloteau, S. 2000, ApJ, 545, 1034

Stassun, K. G., Mathieu, R. D., & Valenti, J. A. 2006, Nature, 440, 311

Terebey, S., Shu, F. H., & Cassen, P. 1984, ApJ, 286, 529

Umbreit, S., Burkert, A., Henning, T., Mikkola, S., & Spurzem, R. 2005, ApJ, 623, 940

Watson, D. M., et al. 2004, ApJS, 154, 391

Watson, A. M., Stapelfeldt, K. R., Wood, K., Ménard, F. 2007, in Protostars & Planets V, eds. B. Reipurth, D. Jewitt, & K. Keil (Univ. Arizona Press: Tucson), 523

White, R. J., & Hillenbrand, L. A. 2004, ApJ, 616, 998

Whitney, B. A., Wood, K., Bjorkman, J. E., & Wolff, M. J. 2003, ApJ, 591, 1049

Wilner, D. J., & Welch, W. J. 1994, ApJ, 427, 898

Wolf, S., Schegerer, A., Beuther, H., Padgett, D. L., & Stapelfeldt, K. R. 2008, ApJ, 674, L101

This preprint was prepared with the AAS LaTeX macros v5.2.

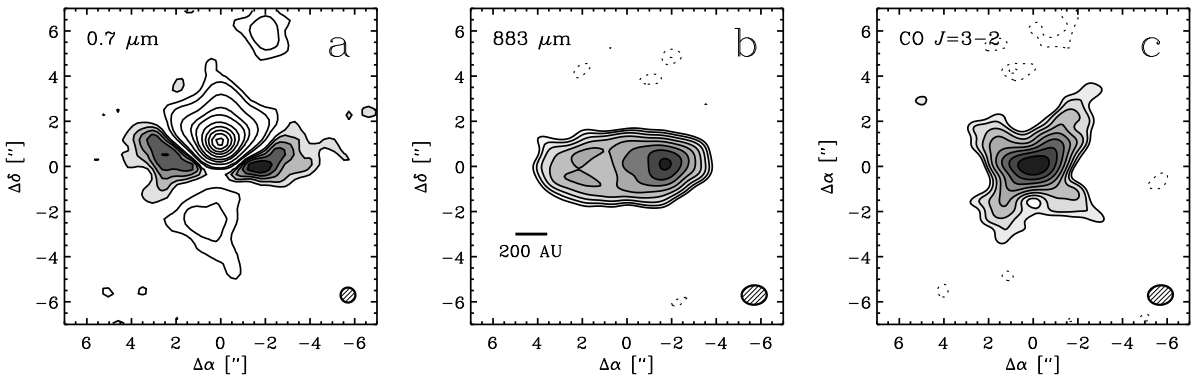

Fig. 1.— Images of the gas and dust surrounding IRAS 04158+2805. (*left*) Optical R-band (0.7 μm) image showing a dark lane in silhouette (grayscale contours; linear steps) against background nebulosity and scattered starlight (unfilled contours; logarithmic steps). (*middle*) Submillimeter (883 μm) dust continuum image from the SMA. Contours start at $3\,\sigma$ ($\sim$3.5 mJy beam^{-1}) and increase by factors of $\sqrt{2}$. (*right*) Velocity-integrated ($0^{\rm th}$ moment) emission image from the CO J=3−2 transition, constructed from 9 spectral channels (a velocity width of 6.3 km s^{-1}). Contours start at $3\,\sigma$ (0.5 Jy km s^{-1} beam^{-1}) and increase by factors of $\sqrt{2}$. Effective FWHM (synthesized) beam sizes are shown in the lower right corner of each panel.

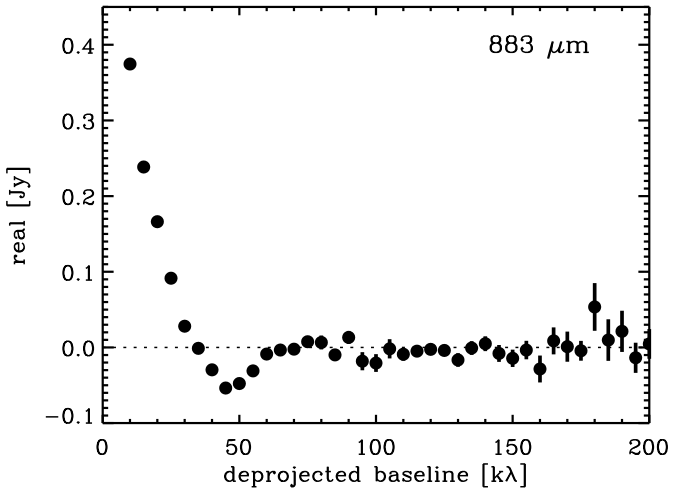

Fig. 2.— The real part of the IRAS 04158+2805 883 μm visibilities as a function of the interferometer baseline, after deprojection and elliptical averaging according to the observed geometry (see Lay et al. 1997). The steep drop in the visibilities at short baselines and the pronounced null at $\sim$30-40 kλ confirm the morphology in Fig. 1b; the submillimeter emission is not centrally peaked.

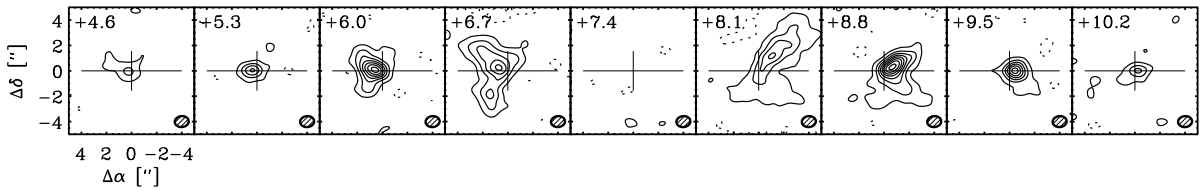

Fig. 3.— Channel maps of the IRAS 04158+2805 CO J=3−2 line emission. Contours start at $3\,\sigma$ (0.2 Jy beam^{-1}) and increase linearly in $6\,\sigma$ increments. The FWHM synthesized beam sizes are shown in the lower right of each panel, and the LSR velocity of each channel (in km s^{-1}) is shown in the upper left. The crosshairs mark the horizontal extent of the submillimeter continuum emission and the vertical extent corresponding to the inclination (62°) derived from fits of the continuum visibilities. There is a clear velocity gradient along the major axis of the continuum emission and optical silhouette.

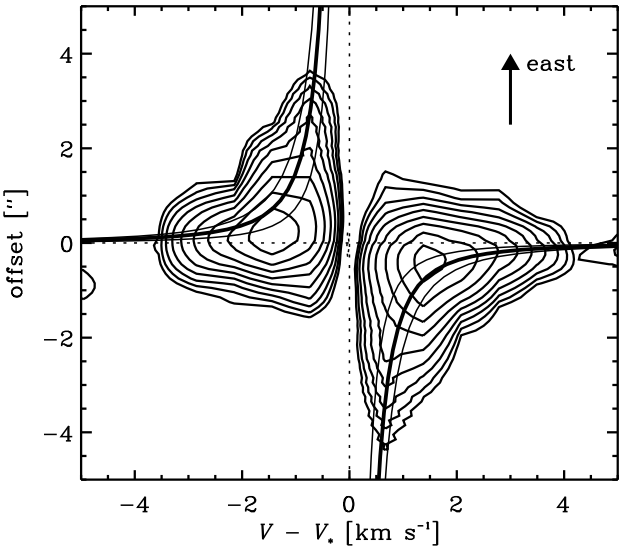

Fig. 4.— Position-velocity diagram of the CO J=3−2 line emission. Contours start at 0.1 Jy and increase in steps of $\sqrt{2}$. The ordinate shows the projected offset from the image center (with positive values to the east), and the abscissa shows the velocity offset from the systemic value, +7.4 km s^{-1}. The heavy curve represents an inclined (i = 62°) Keplerian rotation profile that is most similar to the data, for $M_* = 0.3\,\mathrm{M}_\odot$. Lighter curves on either side show similar profiles for $M_* = 0.15$ and $0.45\,\mathrm{M}_\odot$.

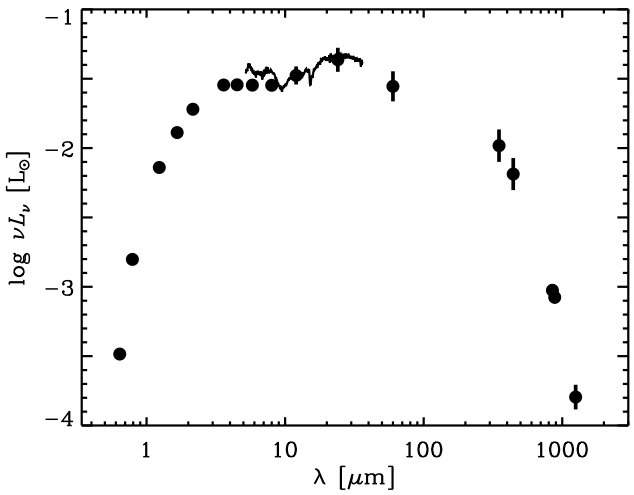

Fig. 5.— The IRAS 04158+2805 spectral energy distribution. Optical photometry was taken from Luhman & Rieke (1998), infrared data from the 2MASS Point Source Catalog (Cutri et al. 2003), Luhman et al. (2006), and Beichman et al. (1986), the mid-infrared *Spitzer* IRS spectrum from Furlan et al. (2008), the submillimeter data from measurements presented here, and the 1.3 mm flux density from Motte & André (2001). See Furlan et al. (2008) for a more detailed discussion of the mid-infrared spectral features.